

Characterization of barrier-tunable radio-frequency-SQUID for Maxwell's demon experiment

Gang Li(李刚), Suman Dhamala, Hao Li(李浩), JianShe Liu(刘建设), Wei Chen(陈炜)
Citation: Chin. Phys. B . 2018, 27(6): 068501. **doi:** 10.1088/1674-1056/27/6/068501

Journal homepage: http://cpb.iphy.ac.cn; http://iopscience.iop.org/cpb

What follows is a list of articles you may be interested in

Modulation depth of series SQUIDs modified by Josephson junction area

Jie Liu(刘杰), He Gao(高鹤), Gang Li(李刚), Zheng Wei Li(李正伟), Kamal Ahmada, Zhang Ying Shan(张颖珊), Jian She Liu(刘建设), Wei Chen(陈炜)
Chin. Phys. B . 2017, 26(9): 098501. **doi:** 10.1088/1674-1056/26/9/098501

Bridge-free fabrication process for Al/AlO_x/Al Josephson junctions

Ke Zhang(张珂), Meng-Meng Li(李蒙蒙), Qiang Liu(刘强), Hai-Feng Yu(于海峰), Yang Yu(于扬)
Chin. Phys. B . 2017, 26(7): 078501. **doi:** 10.1088/1674-1056/26/7/078501

Fabrication of Al/AlO_x/Al junctions using pre-exposure technique at 30-keV e-beam voltage

Dong Lan(兰栋), Guangming Xue(薛光明), Qiang Liu(刘强), Xinsheng Tan(谭新生), Haifeng Yu(于海峰), Yang Yu(于扬)
Chin. Phys. B . 2016, 25(8): 088501. **doi:** 10.1088/1674-1056/25/8/088501

An efficient calibration method for SQUID measurement system using three orthogonal Helmholtz coils

Hua Li(李华), Shu-Lin Zhang(张树林), Chao-Xiang Zhang(张朝祥), Xiang-Yan Kong(孔祥燕), Xiao-Ming Xie(谢晓明)
Chin. Phys. B . 2016, 25(6): 068501. **doi:** 10.1088/1674-1056/25/6/068501

Increasing energy relaxation time of superconducting qubits with nonmagnetic infrared filter and shield

Yuhao Liu(刘宇浩), Mengmeng Li(李蒙蒙), Dong Lan(兰栋), Guangming Xue(薛光明), Xinsheng Tan(谭新生), Haifeng Yu(于海峰), Yang Yu(于扬)
Chin. Phys. B . 2016, 25(5): 058501. **doi:** 10.1088/1674-1056/25/5/058501

Characterization of barrier-tunable radio-frequency-SQUID for Maxwell's demon experiment*

Gang Li(李刚)[1], Suman Dhamala[2], Hao Li(李浩)[1], Jian-She Liu(刘建设)[1], and Wei Chen(陈炜)[1,†]

[1] *Tsinghua National Laboratory for Information Science and Technology, Department of Microelectronics and Nanoelectronics, Institute of Microelectronics, Tsinghua University, Beijing* 100084, *China*

[2] *Department of Physics and Astronomy, University of Kansas, Lawrence, Kansas* 66045, *USA*

(Received 10 January 2018; revised manuscript received 26 March 2018; published online 10 May 2018)

We present the design, fabrication, and characterization of a barrier-tunable superconducting quantum interference device (SQUID) qubit for the study of Maxwell's demon experiment. In this work, a compound Josephson junction (CJJ) radio-frequency (RF)-SQUID qubit with an overdamped resistively shunted direct-current (DC)-SQUID magnetometer is used to continuously monitor the state of the qubit. The circuit is successfully fabricated with the standard Nb/Al-AlO_x/Nb trilayer process of our laboratory and characterized in a low noise measurement system, which is capable of measuring coherent dynamics of superconducting qubits, in an Oxford dilution refrigerator. All circuit parameters are determined accurately by fitting experimental data to theoretical analysis and simulation, which allows us to make a quantitative comparison between the results of the experiment and theory.

Keywords: barrier-tunable RF-SQUID, shunted DC-SQUID, Maxwell's demon

PACS: 85.25.Cp, 85.25.Dq, 07.20.Mc **DOI:** 10.1088/1674-1056/27/6/068501

1. Introduction

Maxwell's demon (MD)[1] is a wizard of wisdom in a thought experiment. It can separate the hot and cold gas molecule in a container box, thus creating a finite temperature difference between the two sides of the box and lowering the entropy of the system, which violates the second law of thermodynamics. However, contemporary studies have shown that the conclusion of this violation is only a paradox, because Maxwell's demon must participate in the thermodynamic cycle as part of the heat engine, whose memory still has the information about the velocity of the molecules. According to Landauer's principle,[2] erasing a bit of information in the equilibrium state requires at least an energy of $k_{\rm B}T\ln 2$ (where $k_{\rm B}$ is the Boltzmann constant and T is the ambient temperature) which is about 3×10^{-21} J. So, even if such a demon does exist, the second law of thermodynamics will not be violated after the erasure of the demon's memory.[3]

Realizing the MD experiment can help us understand the Landauer principle, which would reveal a profound relation between the information content and entropy of a thermodynamic system. In recent years, the majority of studies, both theoretically[3,4] and, in particular, experimentally,[5–9] have been focusing on the classical regime. Raizen *et al.*[9] cooled atoms from 10 mK to 15 μK based on the principle of "Maxwell's demon". Toyabe *et al.*[8] used organic molecules to implement the MD experiment. Koski *et al.*[5,6] realized a Szilard engine[10] in a single-electron box. These experiments demonstrated quantitatively the extraction of heat energy $k_{\rm B}T\ln 2$ by creating a bit of information.

In this paper, a compound Josephson junction (CJJ) radio frequency superconducting quantum interference device (RF-SQUID)[11–14] qubit is designed. An overdamped resistively shunted direct-current (DC)-SQUID[15] is inductively coupled to the qubit to monitor its fluxoid state. According to the description of the MD experiment, to do the experiment we need a particle in a two-state system. In the system the particle can be easily manipulated, depending on its state, and the energy change during the manipulation can be easily calculated.

As a kind of macroscopic qubit, the CJJ RF-SQUID qubit can work as a flux qubit with two quantum states, which can be easily controlled and readout. To obtain the energy change during the experiment, an overdamped DC-SQUID magnetometer instead of unshunted DC-SQUID[16] is used, because it can continuously monitor the state of the RF-SQUID qubit. The purpose of this design is to study the MD experiment on quantum systems.[17–20] In this paper, we mainly describe the design and characterization of the CJJ RF-SQUID qubit. The rest of this paper is arranged as follows. In Section 2, the basic principle of the CJJ RF-SQUID qubit used in the MD experiment is introduced. In Section 3, the design and fabrication process of the qubit are presented. In Section 4, the parameters are determined by fitting the experimental data to theoretical analysis and the potential energy of the qubit is obtained. Some conclusions are drawn from the present study in Section 5, finally.

*Project supported by the National Natural Science Foundation of China (Grant No. 11653001), the National Basic Research Program of China (Grant No. 2011CBA00304), the Tsinghua University Initiative Scientific Research Program, China (Grant No. 20131089314), and the Zhejiang Tianjingsheng Foundation, China, for Student Assistantships (Gang Li and Hao Li).

†Corresponding author. E-mail: weichen@tsinghua.edu.cn

© 2018 Chinese Physical Society and IOP Publishing Ltd

2. Operation principle of demon in qubit

As shown in Fig. 1(a), the CJJ RF-SQUID qubit is an RF-SQUID of loop inductance L with the Josephson junction that is replaced by two Josephson junctions in a small loop of inductance l. In the limit of $l/L \ll 1$ and assuming the two Josephson junctions are identical, the potential energy can be approximated well as[12]

$$U(\phi) = U_0 \left[\frac{1}{2}(\phi - \phi_x)^2 - \frac{\beta_L}{4\pi^2} \cos(2\pi\phi) \right], \tag{1}$$

where $U_0 \equiv \Phi_0^2/L$ and $\beta_L = \beta_{L0}\cos(\pi\phi_{CJJ})$, ϕ is the total flux threading the RF-SQUID loop, ϕ_x and ϕ_{CJJ} are the external flux applied to the RF-SQUID loop and the compound Josephson junction, respectively. All the flux parameters are normalized to the flux quantum $\Phi_0 \equiv h/2e$.

The potential energy is of a double-well as shown in Fig. 1(b). Quantization of fluxoid requires $\phi + \theta/2\pi = n$, $n = 0, \pm1, \pm2, \ldots$. The left and right potential wells in the figure represent the case where the fluxoid is '0' or '1'. When the applied flux $\phi_x = 1/2$, $U(\phi)$ is a symmetric double-well potential, where $\Delta U_L = \Delta U_R$, and if the system is initially placed in, say, state '0' at $t = 0$, after a time t, it could jump to state '1' by incoherent tunneling.[11] The probability with which the system remains in state "0" is given by

$$P(t) = e^{-t/\tau}, \tag{2}$$

where τ is the lifetime of the "0" state. The transition rate between the two wells, $\Gamma = \tau^{-1}$ is given by

$$\Gamma = \frac{\omega_0}{2\pi} \exp\left[-\frac{\Delta U_L}{k_B T} \right]. \tag{3}$$

When the applied flux ϕ_x does not exactly equal $1/2$, the transition rates from "0"-to-"1" and "1"-to-"0" wells are different:

$$\Gamma_{0\to1} = \frac{\omega_{0L}}{2\pi} \exp\left[-\frac{\Delta U_L}{k_B T} \right], \tag{4}$$

$$\Gamma_{1\to0} = \frac{\omega_{0R}}{2\pi} \exp\left[-\frac{\Delta U_R}{k_B T} \right]. \tag{5}$$

We denote the energy difference between the two potential minima, also called the tilt, as $\epsilon = \Delta U_R - \Delta U_L$. For $|\phi_x - 1/2| \ll 1$ the potential tilt ϵ depends on ϕ_x linearly and it can be determined from the transition rate

$$\epsilon = k_B T \ln\left(\frac{\Gamma_{0\to1}}{\Gamma_{1\to0}} \right), \tag{6}$$

where we consider $\omega_{0L} \approx \omega_{0R}$.

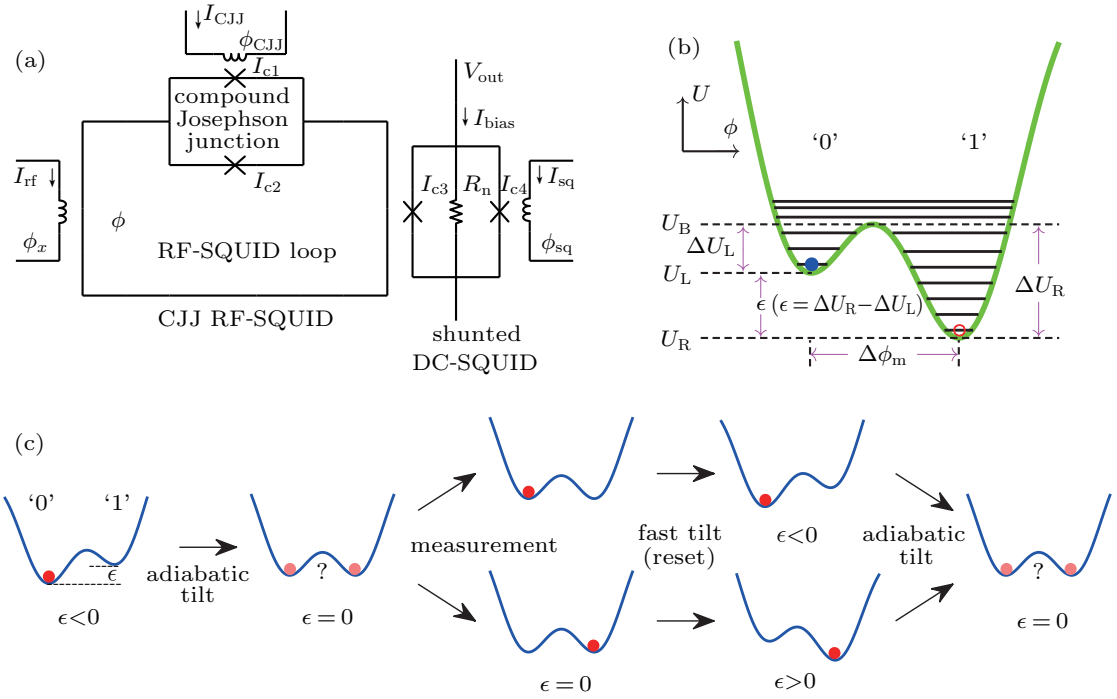


Fig. 1. (color online) (a) Schematic diagram of CJJ RF-SQUID qubit with an overdamped DC-SQUID used to monitor the state of qubit. I_{bias} is the bias current of DC-SQUID. V_{out} is the output voltage of DC-SQUID. ϕ and ϕ_x are the total and external flux applied to the RF-SQUID loop. ϕ_{CJJ} is the external flux applied to the compound Josephson junction. ϕ_{sq} is the external flux applied to the DC-SQUID loop. ϕ_x tilts the potential and ϕ_{CJJ} raises and lowers the barrier between the wells. (b) Potential of the RF-SQUID as a function of ϕ. ΔU_L (ΔU_R) is the barrier seen from the left (right) well and ϵ is the energy difference between the two potential minima (positive in this case). (c) Sketch of energy diagrams for the operation cycle of Maxwell demon.

An ideal operation cycle for the MD experiment is shown in Fig. 1(c). The cycle starts at the potential tilt $\epsilon < 0$ and the qubit state is '0', which lead to zero entropy. The next step of the cycle is a quasi-static tilt which changes the system into the degeneracy ($\epsilon = 0$), due to the incoherent tunneling, the qubit state is uncertain, so the entropy of the system increases by $k_B \ln 2$, corresponding to the heat extracted from the bath, which is equal to Landauer value $Q_L = k_B T \ln 2$. After reach-

ing the degeneracy point, a measurement of the qubit state is performed. If the qubit is in the '0' state, a fast ramp is used and the system is reset to the initial state '0' for the next cycle; if the measured state is '1', the system is fast reset to state '1', which has the same $|\epsilon|$ as the system resetting to initial state '0', for the next cycle. Such a rapid feedback drive traps the qubit to the measured state. Ideally, this drive is so fast that no state change has a chance to occur and, as a result, no heat is transferred to the reservoir.[6]

This process will be repeated many times to obtain the average extracted heat and average work after we have designed a feedback device to realize the MD experiment. Depending on the potential tilt ϵ , the extracted heat and work can be calculated by the following equations step by step:

$$W_i = W_{i-1} - \frac{1}{2} S_i(\epsilon_i - \epsilon_{i-1}), \tag{7}$$

$$Q_i = Q_{i-1} - \frac{1}{2}(S_i - S_{i-1})\left(\frac{\epsilon_i + \epsilon_{i-1}}{2}\right), \tag{8}$$

where S_i and ϵ_i are the state and energy difference at the i-th step, and W_i and Q_i are the total work done by the environment and the heat absorbed from the environment after the i-th step.

3. Design and fabrication

To minimize the effects of ambient magnetic field and cross talks between ϕ_x and $\phi_{\rm CJJ}$, the RF-SQUID loop was designed as a parallel gradiometer[13,21] as shown in Fig. 2(b). The RF-SQUID had the following parameters: $L = 100$ pH, maximum critical current $I_c = 9.8$ μA, which leads to $\beta_{L0} = 2\pi L I_c/\Phi_0 = 3.0$. The overdamped DC-SQUID had the following parameters: $I_0 = 18$ μA, $R_n = 2$ Ω, where I_0 is the critical current of each junction and R_n is the shunt resistance for the DC-SQUID. In order to produce a large change in DC-SQUID output voltage when the qubit jumped from one well to the opposite well, the mutual inductance between the DC-SQUID and RF-SQUID was enhanced using an overlapping structure.

With the help of InductEX,[22] we extracted the inductance and mutual inductances of the system, and the results are listed in Table 1. In this table, $L_{\rm sq}$ is the loop inductance of the DC-SQUID, L is the loop inductance of the RF-SQUID, l is the inductance of the compound Josephson junction, $M_{\rm sq}$ is the mutual inductance between the DC-SQUID and its flux bias line, $M_{\rm rf}$ is the mutual inductance between the RF-SQUID and its flux bias line, $M_{\rm CJJ}$ is the mutual inductance between the compound Josephson junction and its flux bias line, and M is the mutual inductance between the DC-SQUID and the RF-SQUID.

Table 1. Simulation results with InductEX.

Parameters	Simulation results/pH
$L_{\rm sq}$	18.1
L	104
l	7.36
$M_{\rm sq}$	0.66
$M_{\rm rf}$	2.48
$M_{\rm CJJ}$	0.47
M	2.85

The fabrication process included four photolithographic layers as well as several material deposition and etching steps. In our laboratory, we used a 2-inch (1 inch = 2.54 cm) ⟨100⟩ crystalline N-type single-sided polished wafer, which had a 400-nm thick SiO_2 on its surface. The fabrication started with *in situ* deposition of an Nb/Al-AlO_x/Nb trilayer patterned by lift-off. Then, the second lithography determined the junction area on the trilayer film. Then, we deposited the Pt shunt resistance layer by dc sputtering. Before sputtering Pt, a 10-nm thick Ti layer was sputtered to improve adhesion. For the last step, a 300-nm thick Nb wiring layer was deposited and patterned to determine the modulation coil and connection of the resistance. The photograph of the fabricated chip with bonding wires is shown in Fig. 2(a), and the detail of the main part is shown in Fig. 2(b).

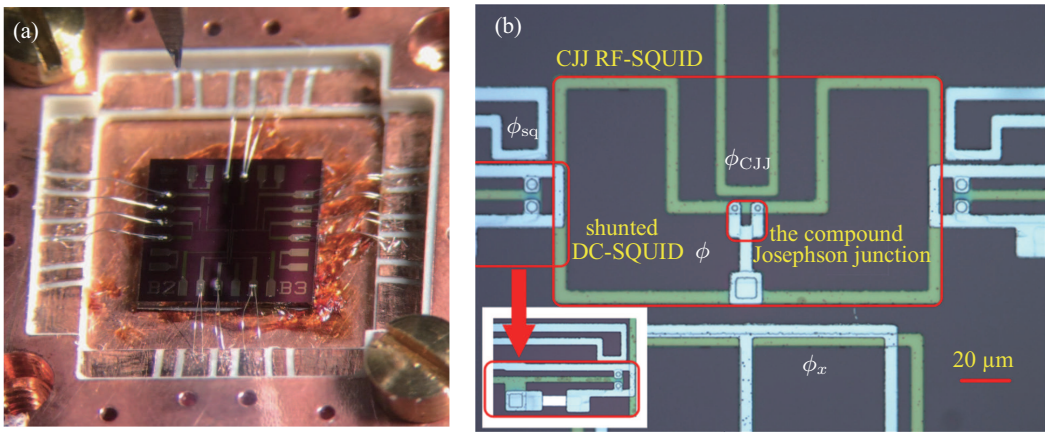


Fig. 2. (color online) (a) Wire bonding and (b) optical micrographs of the SQUID device. Two overdamped dc-SQUIDs are designed, and the left one is used in this paper.

4. Results and discussion

To prepare for the MD experiment, we need to know all relevant parameters of the DC-SQUID and RF-SQUID. The procedure and result are described below. All of the measurements were performed at $T = 4.2$ K.

4.1. Dc-SQUID characterization

Figure 3(a) shows the I–V characteristics of DC-SQUID under different values of flux bias $I_{\rm sq}$. Derived from Fig. 3(a), the switching current of the DC-SQUID $I_{\rm sw}$ is shown in Fig. 3(b), the I–V curves of the DC-SQUID at different values of $\phi_{\rm sq}$ are shown in Figs. 3(c) and 3(d). In this figure,$\phi_{\rm sq}$ is obtained through $I_{\rm sq}$ divided by the period $\Delta I_{\rm sq} = 2968$ μA, from which we obtain $M_{\rm sq} = 0.697$ pH, compared with the extracted value of 0.66 pH from InductEX. As can be seen from this figure, the parameters of the DC-SQUID are $I_0 = 18.5 \pm 0.1$ μA, $R_n = 1.94 \pm 0.18$ Ω and the critical current modulation is $\sim 71.9\%$ of the total critical current. From the modulation depth and comparison with the result in Ref. [23], we can obtain the screening parameter of the DC-SQUID ($\beta_0 = 2L_{\rm sq}I_0/\Phi_0$) to be 0.38 ± 0.01, which leads to a self-inductance $L_{\rm sq} = 21.2 \pm 0.6$ pH. In addition, because of the asymmetry in the inductance of the two arms forming the DC-SQUID loop, $I_{\rm sw}(\phi_{\rm sq})$ is asymmetric and there is a shift between the $I_{\rm sw}$-maxima for opposite-polarity bias current.

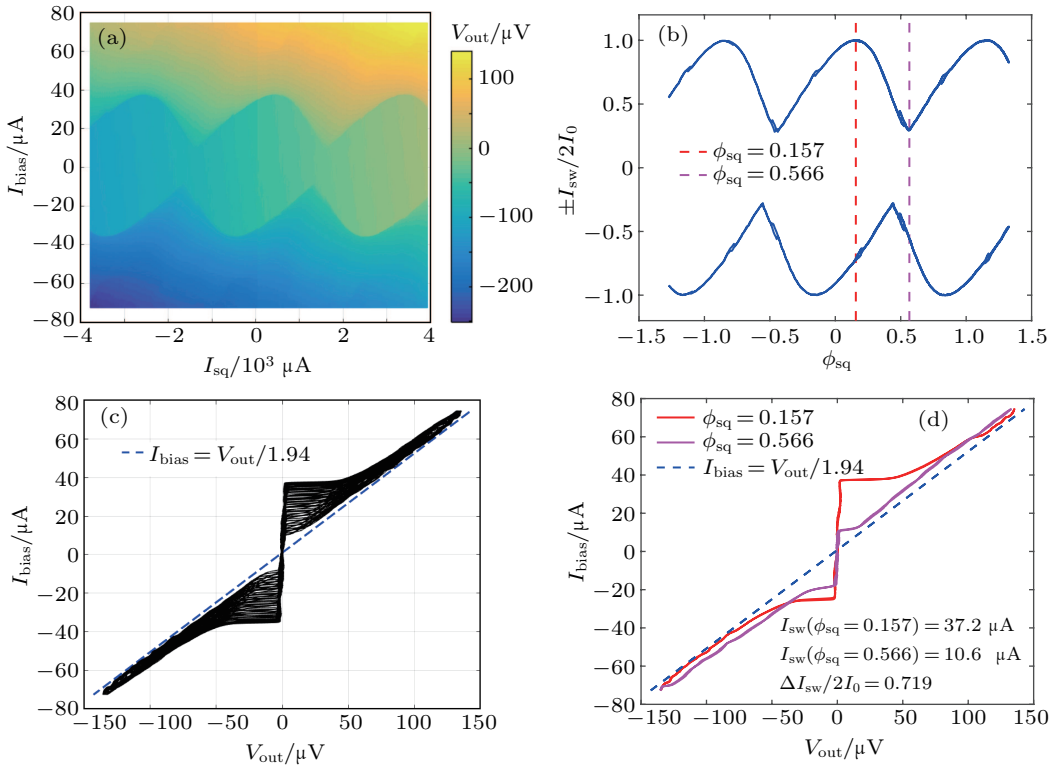


Fig. 3. (color online) (a) DC-SQUID $V_{\rm out}$ under different values of $I_{\rm sq}$ and $I_{\rm bias}$. (b) $I_{\rm sw}(\phi_{\rm sq})$ curve of the DC-SQUID. Here, $\phi_{\rm sq}$ is obtained through $I_{\rm sq}$ divided by period $\Delta I_{\rm sq} = 2968$ μA. $I_{\rm sw}$ is normalized to the critical current of DC-SQUID $2I_0 = 37.0$ μA. (c) I–V curves of DC-SQUID under flux modulation of $\phi_{\rm sq}$. (d) I–V curves of DC-SQUID at $\phi_{\rm sq} = 0.157$ and $\phi_{\rm sq} = 0.566$.

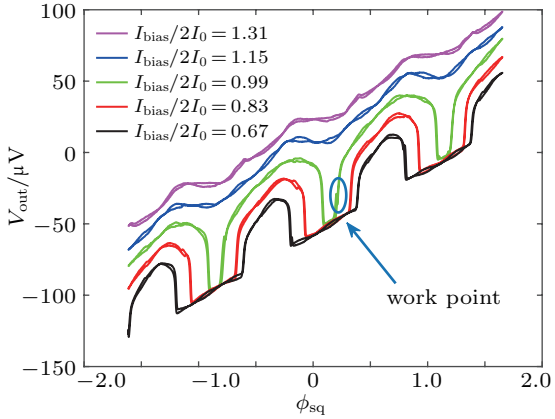


Fig. 4. (color online) DC-SQUID modulation at different values of $I_{\rm bias}$. The blue cycle is the work point used for the readout.

Figure 4 shows the modulation curves versus flux bias $\phi_{\rm sq}$ of DC-SQUID with different values of bias current $I_{\rm bias}$. The bias currents are chosen around the critical current $2I_0$ of DC-SQUID. It can be seen that the DC-SQUID is fluxsensitive near the blue cycle, where we choose the work point for the readout of the RF-SQUID.

4.2. RF-SQUID characterization

By using bias current around $I_{\rm bias}/2I_0 = 0.97$ and adjusting $\phi_{\rm sq}$ around the work point shown in Subsection 4.1, we can maximize the flux sensitivity of DC-SQUID (~ 1040 μV per Φ_0), so that it can clearly distinguish the fluxoid states of the RF-SQUID. Figure 5 shows the RF-SQUID modulation

of ϕ_x under three different values of ϕ_{sq} (1.204 in blue color, 0.206 in red color, and −0.791 in green color), and the difference between two adjacent curves is about one flux quantum Φ_0. In this figure, ϕ_x is obtained through I_{rf} divided by period $\Delta I_{rf} = 865$ μA, from which we can obtain M_{rf} equal to 2.39 pH.

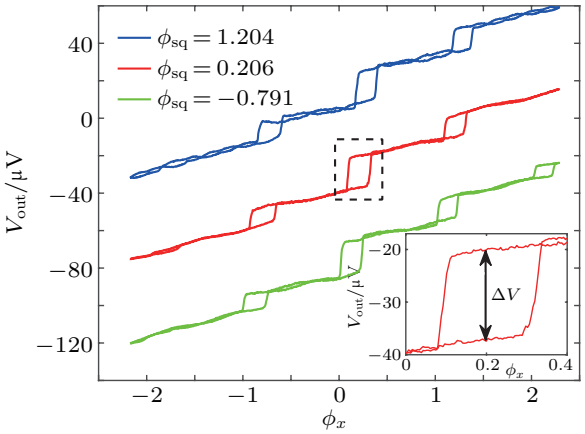


Fig. 5. (color online) RF-SQUID modulations at different values of ϕ_{sq}. ϕ_x is obtained through I_{rf} divided by period $\Delta I_{rf} = 865$ μA. Inset shows the detail of a hysteresis loop in the black frame.

By measuring the width of the hysteresis loop, we can calibrate ϕ_{CJJ}. Figure 6 shows the measured values of loop width along with the curves theoretically calculated from the qubit potential. In this figure, ϕ_{CJJ} is obtained through I_{CJJ} divided by period $\Delta I_{CJJ} = 2984$ μA, from which we can obtain the mutual inductance M_{CJJ} to be equal to 0.69 pH. In the theoretical calculation, the parameters are $L = 120$ pH, $I_c = 9.8$ μA and $\Delta U = 58.0$ K, which can lead to $\beta_{L0} = 3.57$. Additionally, the height of the hysteresis loop at the symmetric point can be used to obtain the mutual inductance between the DC-SQUID and the RF-SQUID according to $M = \Delta\phi_{sq}\Phi_0/\Delta I_s$, where $I_s = \phi\Phi_0/L$ is the circulation current in the RF-SQUID. From the inset of Fig. 5, we can obtain $\Delta V \approx 18$ μV, which can lead to $\Delta\phi_{sq} \approx 0.017$. Based on the dependence of the total flux in the loop ϕ on applied flux ϕ_x (here, ϕ_x of the symmetric point is adjusted to 0.5): $\phi = \phi_x - \beta_{L0}\sin(\phi)$, we can derive that $\Delta I_s \approx 13.4$ μA, so $M \approx 2.62$ pH.

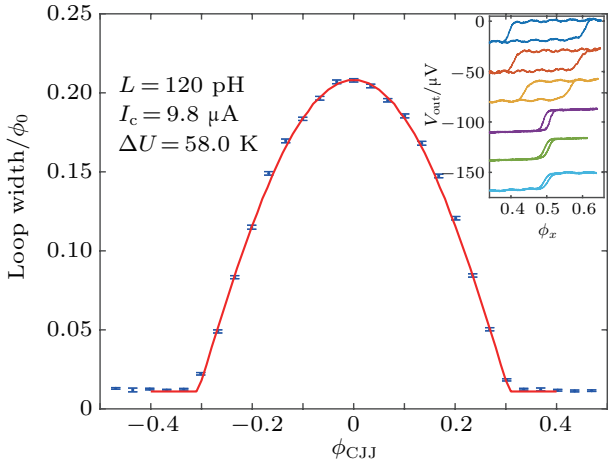


Fig. 6. (color online) Measured width (blue points) of the hysteresis loop as a function of ϕ_{CJJ} along with the theoretical curve (in red color) calculated from the qubit potential for $L = 120$ pH, $I_c = 9.8$ μA, and $\Delta U = 58.0$ K. ϕ_{CJJ} is obtained through I_{CJJ} divided by period $\Delta I_{CJJ} = 2984$ μA. Each point is obtained by averaging 200 repeats at the fixed values of I_{bias} and ϕ_{sq}. The inset shows the measurements of hysteresis loop at different values of ϕ_{CJJ}, here, ϕ_x of the symmetric point is adjusted to 0.5.

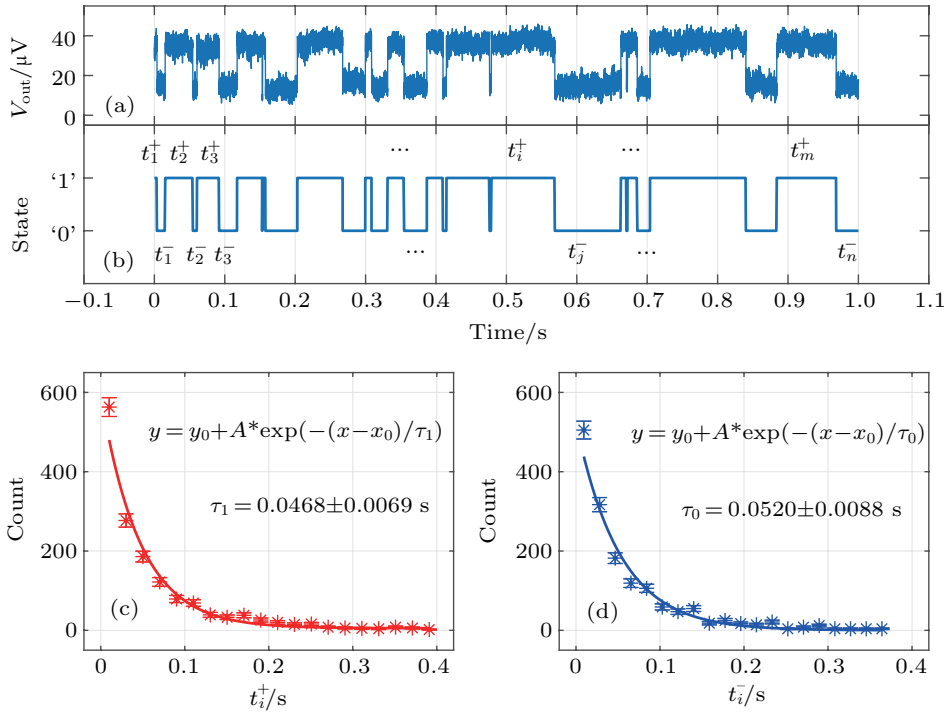


Fig. 7. (color online) (a) Part of the original data of V_{out} measured at $I_{bias}/2I_0 = 0.97$, $\phi_{sq} = 0.206$, $\phi_{CJJ} = -0.268$, and $\phi_x = -0.4984$. (b) Digitized original data. Distribution and exponential fitting of (c) t_i^+ and (d) t_i^-, where t_i^+ and t_i^- are residence times at states '1' and '0', respectively.

4.3. Potential characterization

By setting the bias of ϕ_x to be a fixed value around the symmetric point of the RF-SQUID, and measuring the state of the RF-SQUID in a long time, we can obtain the lifetimes of state '0' (τ_0) and state '1' (τ_1). Figure 7 shows the procedure of extracting τ_0 and τ_1 from a typical time record of DC-SQUID voltage, $V_{\rm out}$. Figure 7(a) shows the original data of $V_{\rm out}$ measured at $I_{\rm bias}/2I_0 = 0.97$, $\phi_{\rm CJJ} = -0.268$, $\phi_{\rm sq} = 0.206$, and $\phi_x = -0.4984$. Figure 7(b) shows the digitized original data. To calculate the lifetime, we obtain the residence time at state '1' (t_i^+) and the residence time at state '0' (t_i^-). Figures 7(c) and 7(d) show the distributions of t_i^+ and t_i^-, and fitting to an exponential function to determine the values of τ_1 and τ_0. In this way we can obtain the lifetimes of states '0' and '1' at a fixed ϕ_x. By changing ϕ_x, and repeating this procedure we can obtain the lifetimes of states '0' and '1' as a function of ϕ_x. The result of $\phi_{\rm CJJ} = -0.268$ is shown in the insert of Fig. 8. From the results of τ_0 and τ_1, we can obtain the energy difference between the values of two potential minima ϵ, which is significant for the MD experiment.

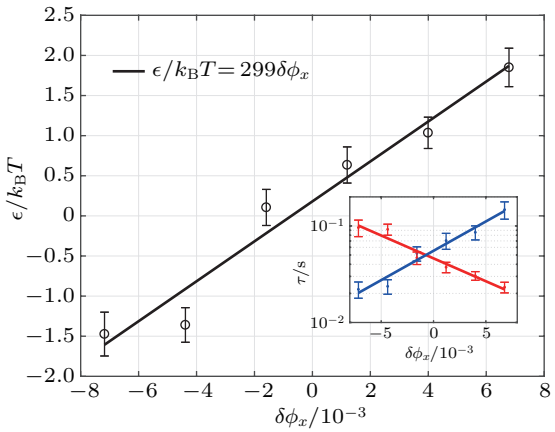


Fig. 8. (color online) Plot of energy difference ϵ/k_BT versus $\delta\phi_x$ (where $\delta\phi_x = \phi_x - 0.5$). Insert shows τ_1 (red) and τ_0 (blue) varying with $\delta\phi_x$ at $\phi_{\rm CJJ} = -0.268$, each point is obtained by the method shown in Fig. 7.

5. Conclusions

The CJJ RF-SQUID with overdamped DC-SQUID for continuous readout have been designed and fabricated successfully using our Nb-based lift-off process. The parameters are simulated by InductEX and verified at low temperature. Moreover, the potential energy of the RF-SQUID at $\phi_{\rm CJJ} = -0.268$ is obtained by monitoring its fluxoid state continuously. These experimental results lay a solid foundation for our next MD experiment.

Acknowledgment

We would like to thank Prof. Siyuan Han for his helpful discussion and experimental instruction.

References

[1] Leff H S and Andrew F 2003 *Rex. Maxwell's demon 2: entropy, classical and quantum information, computing* (Institute of Physics)
[2] Landauer R 1961 *IBM Journal of Research and Development* **5** 183
[3] Brandao F, Horodecki M, Ng N, Oppenheim J and Wehner S 2015 *Proc. Nat. Acad. Sci.* **112** 3275
[4] Liboff R L 1997 *Found. Phys. Lett.* **10** 89
[5] Koski J V, Maisi V F, Sagawa T and Pekola J P 2014 *Phys. Rev. Lett.* **113** 030601
[6] Koski J V, Maisi V F, Pekola J P and Averin D V 2014 *Proc. Natl. Acad. Sci.* **111** 13786
[7] Bérut A, Arakelyan A, Petrosyan A, Ciliberto S, Dillenschneider R and Lutz E 2012 *Nature* **483** 187
[8] Toyabe S, Sagawa T, Ueda M, Muneyuki E and Sano M 2010 *Nat. Phys.* **6** 988
[9] Raizen M G 2009 *Science* **324** 1403
[10] Szilard L 1929 *Zeitschrift für Physik A Hadrons and Nuclei* **53** 840
[11] Han S, Lapointe J and Lukens J 1991 *Phys. Rev. Lett.* **66** 810
[12] Friedman J R, Patel V V, Chen W, Tolpygo S K and Lukens J E 2000 *Nature* **406** 43
[13] Bennett D A, Longobardi L, Patel V, Chen W, Averin D V and Lukens J E 2009 *Quantum Inf. Process.* **8** 217
[14] Harris R, Brito F, Berkley A, Johansson J, Johnson M, Lanting T, Bunyk P, Ladizinsky E, Bumble B and Fung A 2009 *New J. Phys.* **11** 123022
[15] Clarke J and Braginski A I 2006 *The SQUID handbook: Applications of SQUIDs and SQUID systems* (John Wiley & Sons)
[16] Li G, Li H, Liu Q C, Zhao H, Liu J S, Li T F and Chen W 2014 *Cryo. & Supercond.* **42** 1 (in Chinese)
[17] Pekola J P 2015 *Nat. Phys.* **11** 118
[18] Pekola J P, Golubev D S and Averin D V 2016 *Phys. Rev. B* **93** 024501
[19] Braga H C, Rulli C C, de Oliveira T R and Sarandy M S 2014 *Phys. Rev. A* **90** 042338
[20] Lebedev A V, Oehri D, Lesovik G B and Blatter G 2016 *Phys. Rev. A* **94** 052133
[21] Bennett D A, Longobardi L, Patel V, Chen W and Lukens J E 2007 *Supercond. Sci. Tech.* **20** S445
[22] Fourie C J, Wetzstein O, Ortlepp T and Kunert J 2011 *Supercond. Sci. Technol.* **24** 125015
[23] Clarke J and Braginski A I 2005 *The SQUID Handbook: Fundamentals and Technology of SQUIDs and SQUID Systems* p. 46